Mem. Fac. Sci Eng. Shimane Univ.
Series A
40, pp.1-8 (2006)

Influence of Difference in Meshes on Prediction of Shear Band in Clay Specimens under Undrained Compression Loadings Using Finite Element Method

Toshihide SHIBI[1)], Takeshi KAMEI[1)] and Yuka HORI[2)]

[1)]*Department of Geoscience, Interdisciplinary Faculty of Science and Engineering, Shimane University*

[2)]*Department of Geoscience, Interdisciplinary Faculty of Science and Engineering, Graduate School of Shimane University*

Abstract

In unconfined compression tests, a clay specimen deforms uniformly at the beginning of loading, but the deformation changes into non-uniform deformation near maximum load. At that time, strain is localized in the specimen, and localization of strain leads to failure of specimens through formation of shear bands. In this study, this phenomenon was detected by using soil-water coupled finite element analysis based on finite strain. Several finite element meshes were used to examine the influence of the three differing mesh sizes on the analytical results. The mechanism of deformation from initiation of strain localization to formation of shear band is simulated using finite element analysis. The inclination angles of the shear bands based on the results of finite element analysis agree well, regardless of differing mesh sizes. Differing meshes influence the width of shear bands and the percentage of shear strain at the shear bands.

1. Introduction

In element tests such as unconfined compression tests and triaxial compression tests, ideally, clay specimens deform uniformly from the beginning of loading through to failure of the specimens (see Fig. 1). In general, deformation of clay specimens is uniform in the early stage of loading. However, deformation changes from uniform deformation to non-uniform deformation near maximum load. Localization of strain then leads to failure of specimens through formation of shear bands. Therefore, signs of failure including shear band formation, localization of strain, and non-uniform deformation appear on the specimens before destruction.

For the sake of simplicity, this phenomenon has been extensively studied under plane strain loading conditions. Morgenstern and Tchalenko (1967) studied the behavior of thin sections of carbowax-impregnated clay in a direct shear device. The implication of the plastic bifurcation for geomechanics has been realized in a number of constitutive models and theoretical bifurcation analyses (e.g. Vardoulakis, 1981;Yatomi *et al*., 1989; Chau and Rudnicki, 1990; Shibi *et al*., 2000). Although stress states and strain distributions are supported by bifurcation analyses when a specimen is deformed non-uniformly, these analyses cannot simulate the following deformation. Using finite element method is useful to simulate non-uniform deformation. Deformation analysis and numerical bifurcation analysis using finite element method have been conducted extensively (e.g. Asaoka and Noda, 1995; Larsson *et al*., 1996; Kobayashi *et al*., 1999).

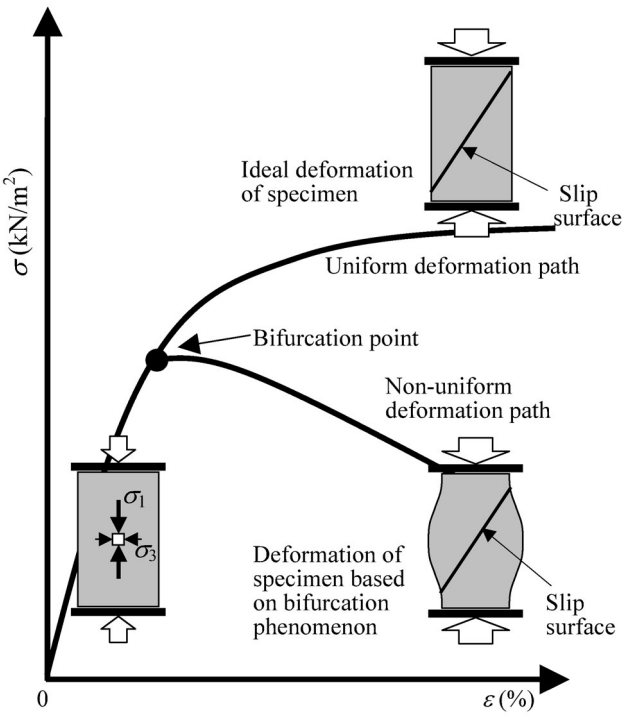

Fig. 1 Stress-strain curve in element test and a concept of bifurcation phenomenon

In this paper, the initiation and propagation of strain localization that developed in rectangular block specimens of

normally consolidated clay during undrained shear under plane strain loading conditions was detected using soil-water coupled finite element analysis based on finite strain. A Cam-clay model was applied for a constitutive equation of clay. A very small scratch was made at a corner of the specimens to facilitate localization of strain. Several finite element meshes of differing size were used to examine the influence of the difference of meshes on the analytical results.

2. Constitutive relation

In this paper, we employ the Cam-clay model for finite deformation (e.g. Roscoe *et al*., 1963; Yatomi *et al*., 1989). The Cam-clay model is known world-wide, and provides a reasonable match with the experimentally observed behavior of saturated clay, even though only a few soil parameters are used. Although there are some sophisticated models than the Cam-clay model, they are complicated and need a lot of parameters. It is desirable for deformation analysis to be comparatively easily carried out precisely quickly from an engineering viewpoint. In this purpose, a comparatively simple model of soil like a Cam-clay model is suitable. The Cam-clay model is summarized briefly below.

It has been well recognized that the constitutive relations for saturated clays should be based on the effective (Cauchy) stress tensor T'_{ij}, which is defined by

$$T'_{ij} = T_{ij} + u\delta_{ij}. \tag{1}$$

Here, T_{ij} is the total Cauchy stress tensor, u is the pore water pressure, and δ_{ij} is Kronecker's delta. Then, the effective mean nominal stress p' and the generalized stress deviator q are defined as

$$p' = -\frac{1}{3}T'_{ii}, \quad q = \sqrt{\frac{3}{2}S_{ij}S_{ij}}, \tag{2}$$

respectively, where S_{ij} is the deviatoric part of T'_{ij}.

Note that, here and in what follows, we regard tension and extension positive and compression and contraction negative except u, p', and the volumetric strain v; an ordinary exchange of the sign in soil mechanics needs a special care and makes the discussion troublesome since stress rates employed in finite strain theory are not merely the rate of stress.

The yield function of the Cam-clay model is of the form

$$F = \frac{\lambda-\kappa}{1+e_0}\ln\frac{p'}{p'_0} + D\frac{q}{p'} - v^{\mathrm{p}} = 0, \tag{3}$$

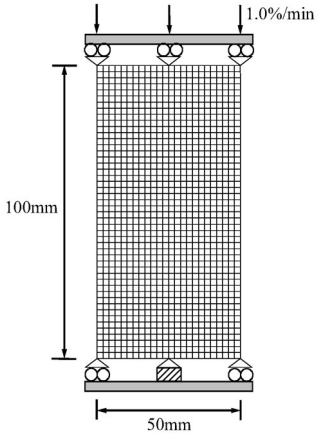

Fig. 2 Boundary condition in the present finite element analysis

where λ and κ are the compression index and the swelling index respectively, e_0 is the void ratio at the initial state, p'_0 is the mean effective stress at the initial state, and D is the coefficient of dilatancy, which is related to the critical state parameter M as defined by $D=(\lambda-\kappa)/\{M(1+e_0)\}$ (e. g. Shibata, 1963; Sekiguchi and Ohta, 1977).

The plastic part of stretching tensor D^{p}_{ij} is expressed by a flow theory as

$$D^{\mathrm{p}}_{ij} = \frac{1}{h}\{\frac{1}{2}\frac{S_{ij}}{\bar{\tau}} - \frac{1}{3}\bar{\beta}\delta_{ij}\}\{\frac{1}{2}\frac{S_{k\lambda}}{\bar{\tau}} - \frac{1}{3}\bar{\beta}\delta_{k\lambda}\}\overset{\circ}{T}'_{k\lambda}, \tag{4}$$

with $\bar{\tau} = \sqrt{S_{ij}S_{ij}/2}$ and $\bar{\beta} = (M - q/p')/\sqrt{3}$, and $h = p'\bar{\beta}/(\sqrt{3}D)$ is the hardening modulus.

The Cam-clay constitutive relation is expressed as

$$\overset{\circ}{T}'_{ij} = \{(\tilde{K} - \frac{2}{3}\tilde{G})\delta_{ij}\delta_{k\lambda} + \tilde{G}(\delta_{ik}\delta_{j\lambda} + \delta_{i\lambda}\delta_{jk}) - \frac{1}{\tilde{G}+\tilde{h}}(\frac{\tilde{G}}{\bar{\tau}}S_{ij} + \tilde{K}\bar{\beta}\delta_{ij})(\frac{\tilde{G}}{\bar{\tau}}S_{k\lambda} + \tilde{K}\bar{\beta}\delta_{k\lambda})\}D_{k\lambda}, \tag{5}$$

where $\tilde{K}(=(1+e)p'/\kappa)$ is the bulk modulus and $\tilde{G}(=3(1-2\nu)\tilde{K}/\{2(1+\nu)\})$ is the shear modulus, where ν is Poisson's ratio.

3. Finite element analysis for shear band formation

The following section presents the numerical results obtained on shear band formation of rectangular clay block under plane strain compression loadings. The objective of this section is to investigate that the mechanism of deformation from initiation of strain localization to formation of shear band was demonstrated by using finite element method.

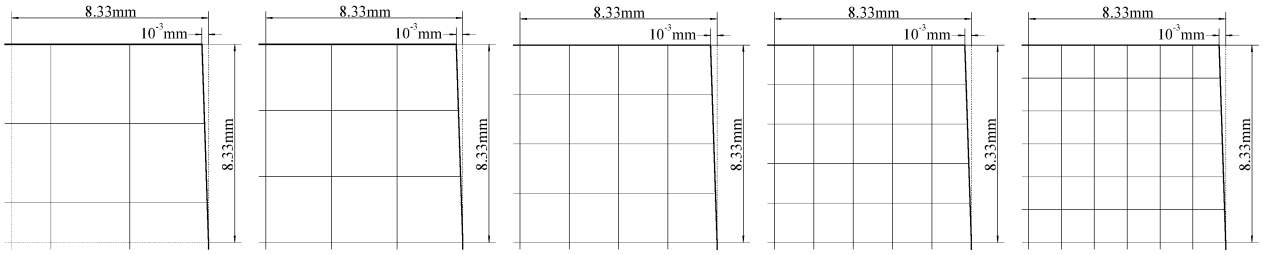

(a) the coarsest mesh (450 elements) (b) coarser mesh (648 elements) (c) medium mesh (1152 elements) (d) finer mesh (1800 elements) (e) the finest mesh (2592 elements)

Fig. 3 Initial imperfection at a right top corner

3.1 Finite Element Method, Boundary Conditions and Their Modeling

The finite element program used in this study was coded according to the method proposed by Sandhu and Wilson (1969). The type of solid element used for deformation was a second order iso-parametric plane strain element with 8 nodal points, and a first order iso-parametric element with 4 nodal points was used for pore water pressure. The analysis with these elements results in better precision than that with lower order elements, such as constant strain triangular element. Using these elements can reduce the number of nodal point and shorten analytical time accordingly.

We consider a rectangular clay specimen with initial width B_0 = 50 mm and with initial height H_0 = 100 mm shown in Fig. 2. The specimen is subjected to plane strain condition. The specimen is discretized into 15 x 30 (=480, the coarsest mesh), 18 x 36 (= 648, coarser mesh), 24 x 48 (=1152, medium mesh), 30 x 60 (=1800, finer mesh), and 36 x 72 (=2592, the finest mesh) elements of equal size to examine the influence of the difference of meshes on the analytical results. As shown in Fig. 2 the top and bottom ends of the specimen are frictionless, while the side face is free. On the top boundary, the displacement is prescribed in the vertical direction and is free in the horizontal direction. The bottom boundary is fixed only the vertical direction, such that the horizontal displacement is allowed. But the center of bottom is fixed to restrict a rigid motion. Concerning the drainage conditions, the boundary of specimen is assumed to be undrained. An initial imperfection, such as a very small scratch, was made at a top right corner of the specimens to facilitate localization of strain (see Fig. 3). In laboratory tests, scratches were made easily at corners of the specimen by accident.

The clay specimen is in a normally consolidated state. Here and in what follows, the soil parameters of the specimen

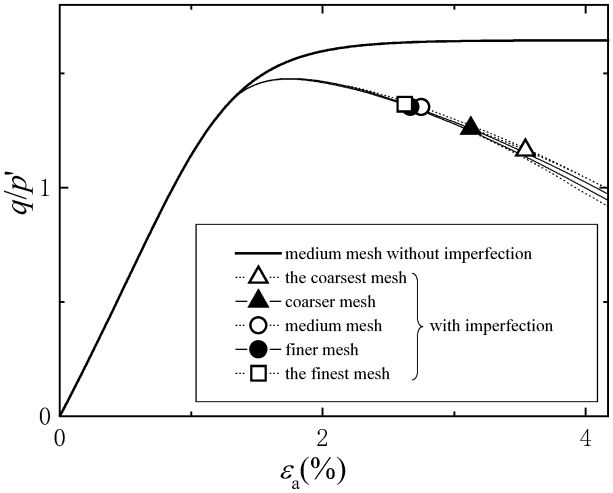

Fig. 4 Stress ratio-strain curves

are taken to be λ = 0.155, κ = 0.021, ν = 0.333, M = 1.650, and e_0 = 1.087 which were determined from experimental results from triaxial tests on Kawasaki Clay, as reported by Nakase and Kamei (1983) and Nakase *et al.* (1988). The coefficient of permeability which is used in the finite element program were assumed to be $k = 1.0 \times 10^{-9}$m/s.

3.2 Numerical results based on finite element method and discussions

We call the stress ratio-strain curve of an ideal specimen without imperfection the main path and this curve is shown in Fig. 4. The main path computed using all meshes agreed, and we illustrate only the main path for medium mesh. In the main path, the stress ratio increased rapidly with increasing an axial strain at the beginning of loading. The stress ratio increased consistently, but its increment quantity gradually decreased when the axial strain exceeded 1%. The ideal specimen was compressed uniformly during loading, and no localization of strain occurred. Curves of specimens with initial imperfection are also shown in Fig. 4. The stress ratio-strain curves of the specimen with initial imperfection are here called the

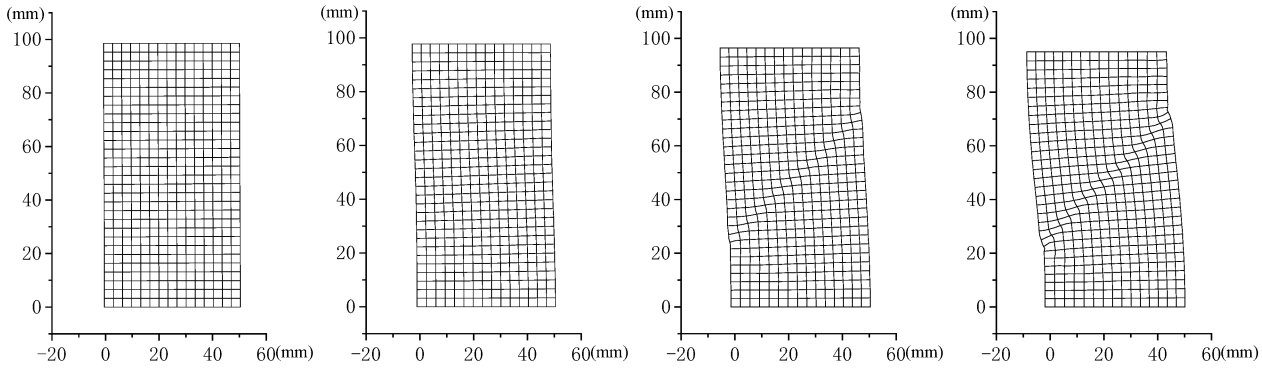

(a) ε_a = 1.46% (b) ε_a = 2.29% (c) ε_a = 3.54% (d) ε_a = 5.00%

Fig. 5 Process of deformation using the coarsest mesh

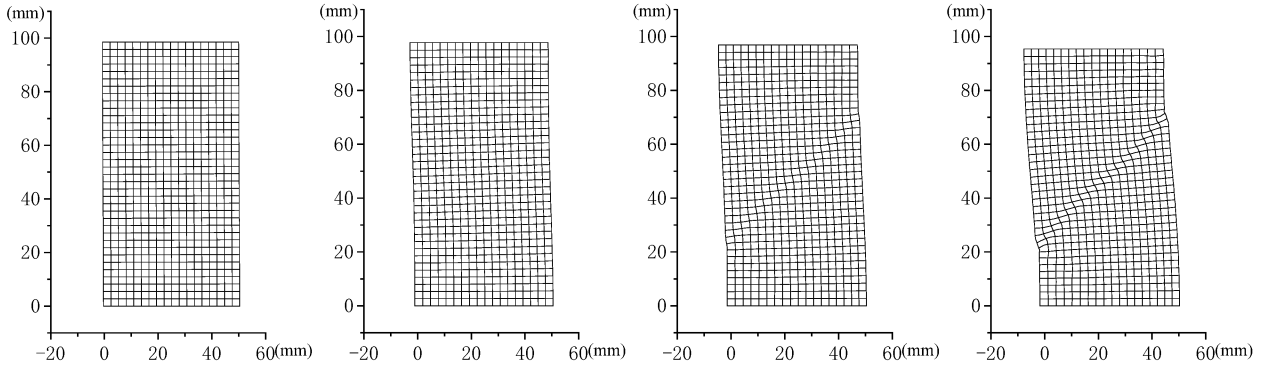

(a) ε_a = 1.46% (b) ε_a = 2.29% (c) ε_a = 3.13% (d) ε_a = 4.38%

Fig. 6 Process of deformation using coarser mesh

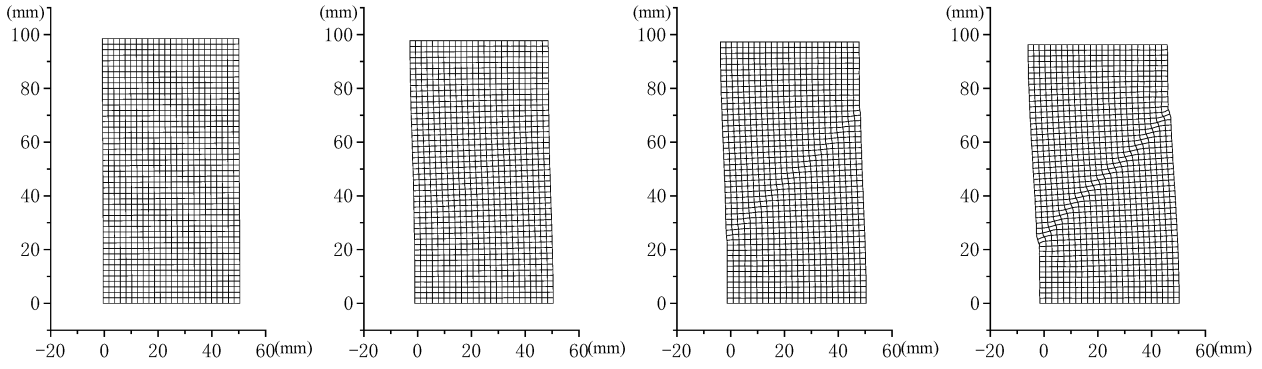

(a) ε_a = 1.46% (b) ε_a = 2.29% (c) ε_a = 2.75% (d) ε_a = 3.75%

Fig. 7 Process of deformation using medium mesh

bifurcation path. The bifurcation paths almost correspond with the main path up to an axial strain of 1.4%. After peaking at an axial strain of 2.0%, the stress ratio gradually decreased. There is no significant mesh size dependency on the stress ratio-strain curves. The value of q/p' of specimen with imperfection at peak was underestimated by 21% compared to that of the ideal specimen. This shows that specimens may only reach 79% of the maximum strength when the initial imperfections exist.

Figures 5~9 show processes of deformation of clay specimen with the coarsest, coarser, medium, finer, and the finest meshes. Specimens were compressed uniformly up to ε_a = 1.46%. When the specimens were compressed further and axial strain increased, their upper parts moved slightly to the left. The deformation of the specimen then changed from uniform deformation to non-uniform deformation at axial strains over 2.29%. In the coarsest mesh, slip surface was observed clearly as localized deformation of finite meshes at ε_a = 5.00%. Slip surface was formed with smaller axial strain as meshes became finer. In the finest mesh, slip surface was observed clearly at ε_a = 3.54%.

In the specimen, localization of strain must have occurred before the localization of deformation. To investigate the localization of strain, transitions of maximum shear strain

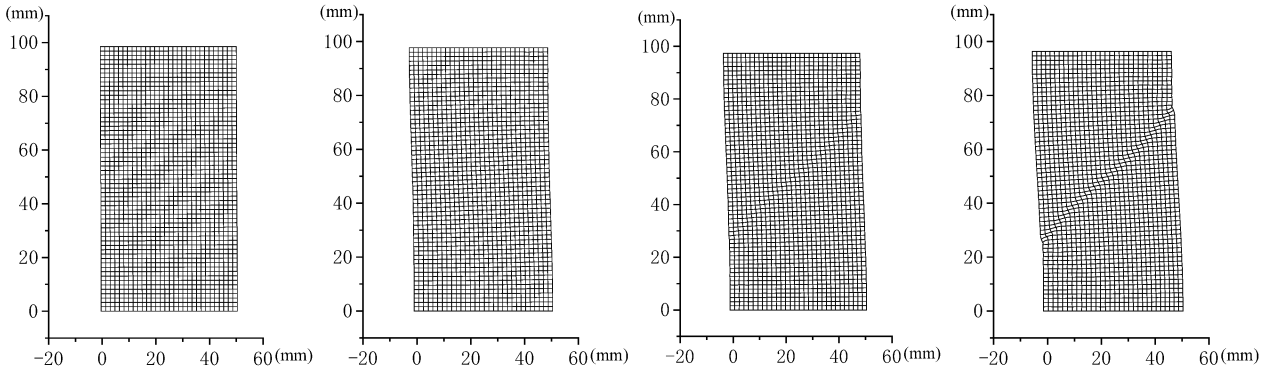

(a) ε_a = 1.46% (b) ε_a = 2.29% (c) ε_a = 2.67% (d) ε_a = 3.67%

Fig. 8 Process of deformation using finer mesh

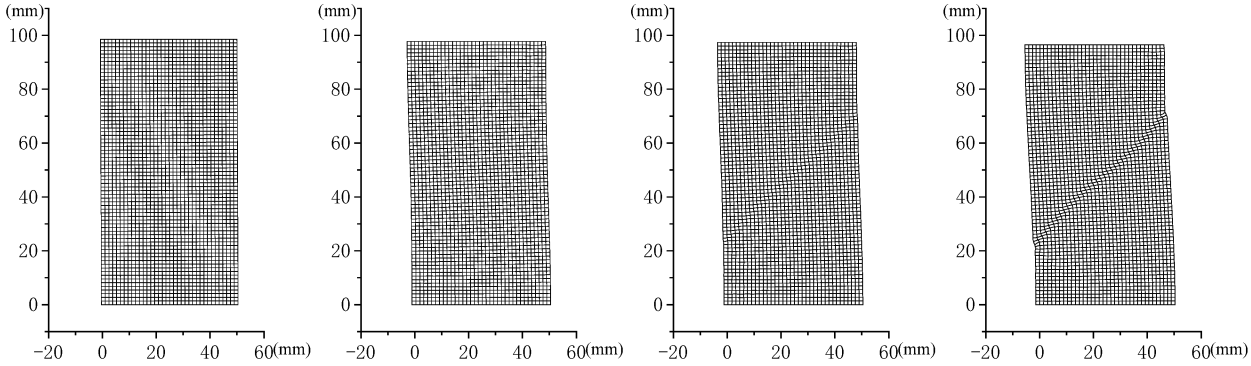

(a) ε_a = 1.46% (b) ε_a = 2.29% (c) ε_a = 2.63% (d) ε_a = 3.54%

Fig. 9 Process of deformation using the finest mesh

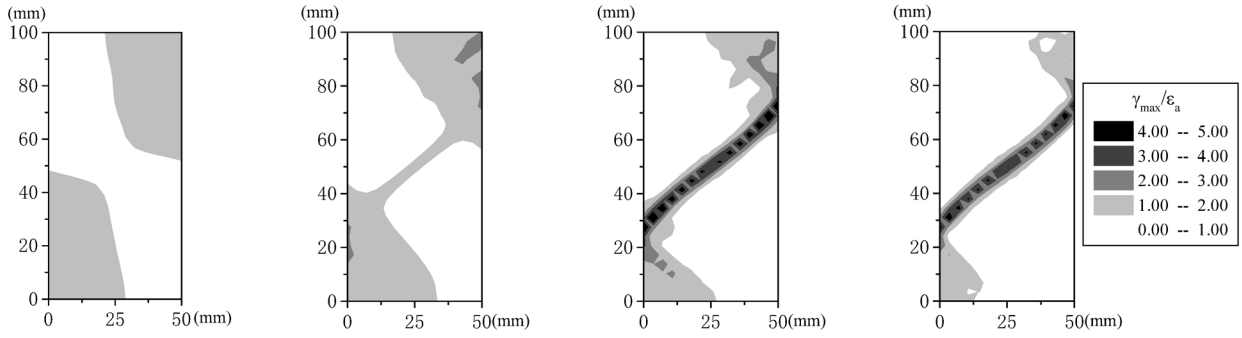

(a) ε_a = 1.46% (b) ε_a = 2.29% (c) ε_a = 3.54% (d) ε_a = 5.00%

Fig. 10 Transition of maximum shear strain contour using the coarsest mesh

contour using each mesh are shown in Figs. 10~14. The maximum shear strain, γ_{max}, is normalized using the axial strain, because the localization of strain results from the distribution of strain in the specimen. In these figures, it is apparent that the maximum shear strain locally increased in the right top and left lower corners of the specimen at axial strain of 1.46%, which seemed to be the uniform deformation from Figs. 5~9. This phenomenon was promoted by the presence of imperfection. In each mesh, localized regions of strain of $\gamma_{max}/\varepsilon_a$ = 1.0~2.0 were connected by a band at ε_a = 2.29%. The value of $\gamma_{max}/\varepsilon_a$ in the banded zone increased markedly with an increasing axial strain. The widths of the banded zone for the coarsest and coarser mesh were greater than those of medium, finer and the fine mesh. The banded zone of $\gamma_{max}/\varepsilon_a$ = 3.0 was formed at $\varepsilon_a \approx$ 2.7% in medium, finer and the finest mesh, and was recognized as shear band formation. In the coarsest and coarser mesh, the shear band was formed later and was observed at ε_a = 3.1 ~ 3.5%. Although the axial strain at which shear band was formed decreased when mesh became finer, its increment quantity gradually decreased when mesh became finer than medium mesh. However, the inclination angles of the shear band in all three cases agreed well, regardless of the differing mesh sizes. The shear bands were formed without passing through the

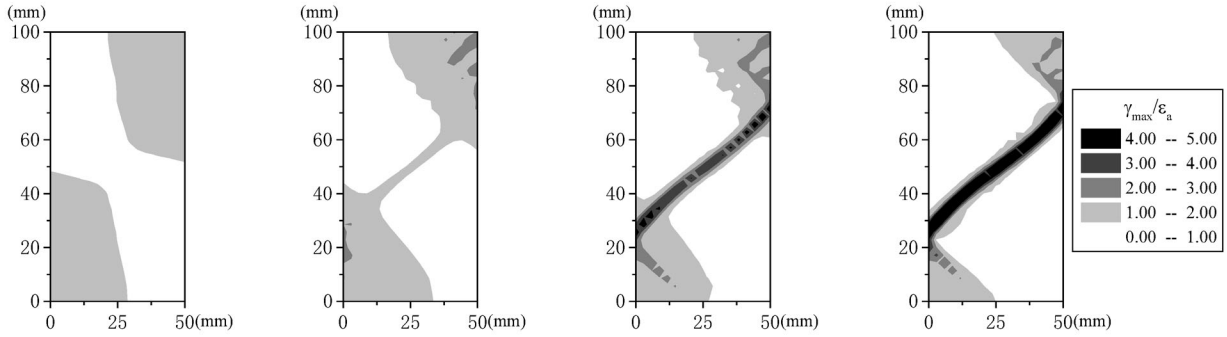

(a) ε_a = 1.46% (b) ε_a = 2.29% (c) ε_a = 3.13% (d) ε_a = 4.38%

Fig. 11 Transition of maximum shear strain contour using coarser mesh

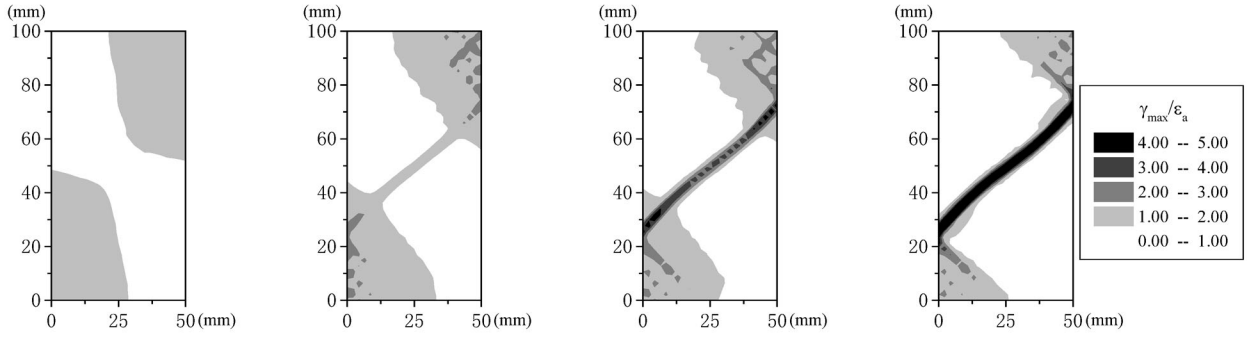

(a) ε_a = 1.46% (b) ε_a = 2.29% (c) ε_a = 2.75% (d) ε_a = 3.75%

Fig. 12 Transition of maximum shear strain contour using medium mesh

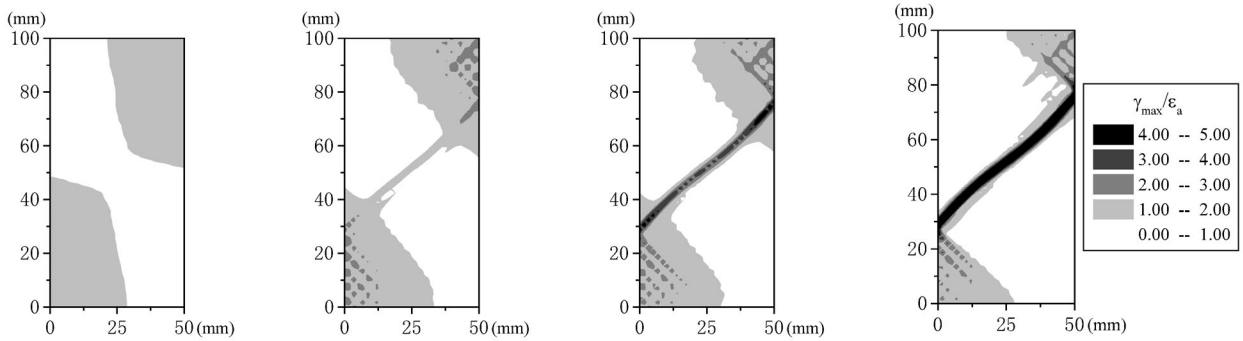

(a) ε_a = 1.46% (b) ε_a = 2.29% (c) ε_a = 2.67% (d) ε_a = 3.67%

Fig. 13 Transition of maximum shear strain contour using finer mesh

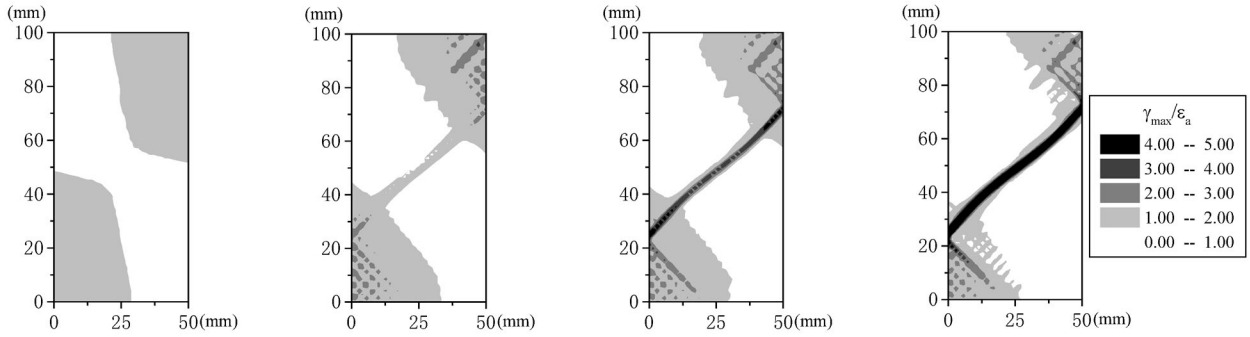

(a) ε_a = 1.46% (b) ε_a = 2.29% (c) ε_a = 2.63% (d) ε_a = 3.54%

Fig. 14 Transition of maximum shear strain contour using the finest mesh

imperfection, and hence the position of the scratch scarcely influenced the position of the shear bands. In the coarsest and coarser mesh, the value of $\gamma_{max}/\varepsilon_a$ in the banded zone increased slowly because the banded zone of strain

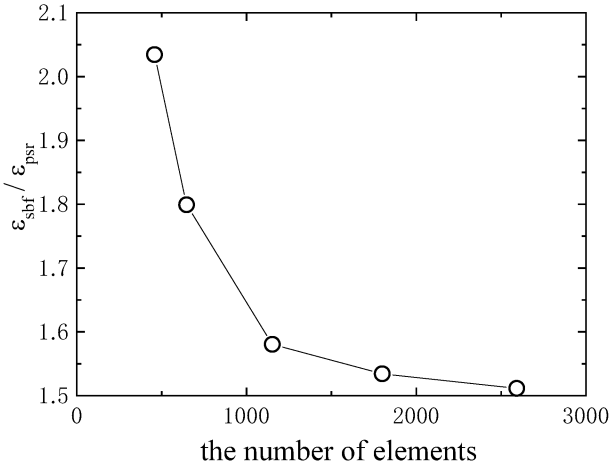

Fig. 15 relationship between ε_{sbf} / ε_{psr} and the number of elements

localization formed was broad. The shear band resulting from medium mesh almost corresponded with that of finer and the finest mesh. Consequently, simulation of clear shear bands can be made by making the mesh sufficiently fine. In this analysis it was sufficient if the specimen was discretized into 24 x 48 elements.

To investigate influence axial strain at which shear band was formed (ε_{sbf}) on differing mesh sizes, relationship normalized by axial strain at the peak of stress ratio (ε_{psr}) and the number of elements is shown in Fig. 15. Although the value of ε_{sbf} / ε_{psr} decreased markedly with an increasing the number of elements, its increment quantity gradually decreased when the number of elements exceeded 1500. It is non-effective to divide a specimen with the number of element more than 1500 because analytical time gets longer when the number of element increases.

In the viewpoint of balance between shortening of an analytical time and precision of an analysis result, it was sufficient if the specimen was discretized into 24 x 48 elements in this analysis

4. Conclusions

The mechanism of deformation from initiation of strain localization to formation of shear band was simulated using finite element analysis. The inclination angles of the shear bands based on the results of finite element analysis agreed well, regardless of differing mesh sizes. Differing meshes influenced the width of shear bands and the percentage of shear strain at the shear bands.

ACKNOWLEDGEMENTS

The authors would like to express their gratitude to Dr. B. P. Roser of Shimane University for his careful proofreading of this paper.

REFERENCES

Asaoka, A. and Noda, T. (1995). "Imperfection-Sensitive Bifurcation of Cam-Clay under Plane Strain Compression with Undrained Boundaries," *Soils and Foundations*, Vol 35, No 1, pp 83-100.

Chau, K. T. and Rudnicki, J. W. (1990). "Bifurcations of Compressible Pressure-Sensitive Materials in Plane-Strain Tension and Compression," *Journal of the Mechanics and Physics of Solids*, Vol 38, No 6, pp 875-898.

Kobayashi, I., Iizuka, A. and Ohta, H. (1999). "The Transition of Localized Deformation Mode Developing in the Normally Consolidated Clay Specimen," *Japan Society of Civil Engineers*, No 617, III-35, pp 147-157 (in Japanese).

Larsson, R., Runesson, K. and Sture, S. (1996). "Embedded Localization Band in Undrained Soil Based on Regularized Strong Discontinuity – Theory and FE-Analysis," *International Journal of Solids and Structures*, Vol 33, No 20-22, pp 3081-3101.

Morgenstern, N. R. and Tchalenko, J. S. (1967). "Microscopic Structures in Kaolin Subjected to Direct Shear," *Geotechnique*, Vol 17, pp 309-327.

Nakase, A. and Kamei, T. (1983). "Undrained Shear Strength Anisotropy of Normally Consolidated Cohesive Soils," *Soils and Foundations*, Vol 23, No 1, pp 91-101.

Nakase, A., Kamei, T. and Kusakabe, O. (1988). "Constitutive Parameters Estimated by Plasticity Index," *Journal of Geotechnical Engineering*, *ASCE*, Vol 114, No 7, pp 844-858.

Roscoe, K. H., Schofield, A. N. and Thurairajah, A. (1963). "Yielding of Clays in States Wetter than Critical," *Geotechnique*, Vol 13, pp 211-240.

Sandhu, R. S. and Wilson, E. L. (1969). "Finite Element Analysis of Flow in Saturated Porous Media," *Journal of the Engineering Mechanics Division*, *ASCE*, Vol 95, No EM3, pp 641-652.

Sekiguchi, H. and Ohta, H. (1977). "Induced Anisotropy and Time Dependency in Clays," *Proceedings of 9th International Conference on Soil Mechanics and Foundation Engineering*, Tokyo, Vol 1, pp 229-238.

Shibata, T. (1963). "On the Volume Changes of Normally-Consolidated Clays," *Disaster Prevention Research Institute*, Kyoto University, No 6, pp 128-134 (in Japanese).

Shibi, T. and Yatomi, C. and Kamei, T. (2000). "Influences of Aspect Ratio on Bifurcation Analysis for a Normally Consolidated Clay under the Plane Strain Undrained Compression Loadings," *Japan Society of Civil Engineers*, No 666, III-53, pp 181-192 (in Japanese).

Vardoulakis, I. (1981). "Bifurcation Analysis of the Plane Rectilinear Deformation on Dry Sand Samples," *International Journal of Solids and Structures*, Vol 17, No 11, pp 1085-1101.

Yatomi, C., Yashima, A., Iizuka, A. and Sano, I. (1989). "General Theory of Shear Bands Formation by a Non-Coaxial Cam-Clay Model," *Soils and Foundations*, Vol 29, No 3, pp 41-53.